



Elucidation of structural, morphological, optical and photoluminescence properties of single and (In, Ga) co-doped ZnO nanocrystalline thin films

M SHAHEERA^{1,*} , K G GIRIJA², MANMEET KAUR³, V GEETHA¹, A K DEBNATH³,
R K VATSA², K P MUTHE³ and S C GADKARI³

¹Research Department of Physics, Government Victoria College, Palakkad 678001, India

²Chemistry Division, Bhabha Atomic Research Centre, Mumbai 400094, India

³Technical Physics Division, Bhabha Atomic Research Centre, Mumbai 400094, India

*Author for correspondence (kcmshahi@gmail.com)

MS received 29 October 2018; accepted 27 February 2019; published online 11 September 2019

Abstract. Single and co-doped ZnO thin films are currently under intense investigation and development for optoelectronic applications. Here in this study, pristine, indium-doped (IZO), gallium-doped (GZO) and co-doped (IGZO) ZnO thin films were deposited on a glass substrate using radio frequency magnetron sputtering. A comparative study of all the films was carried out on the basis of their various properties. The effect of single and co-doping on the structural (X-ray diffraction (XRD) studies and Raman studies), morphological (field emission scanning electron microscopy and energy dispersive X-ray spectroscopy studies) and optical properties (ultraviolet–visible (UV–Vis) and photoluminescence (PL)) of the deposited films was investigated. X-ray photoelectron spectroscopy (XPS) characterization was employed to analyse the surface chemical composition and bonding of the deposited film. From the XRD patterns, it was found that the films were highly crystalline in nature and preferentially oriented along the (002) direction with a hexagonal wurtzite structure, consistent with Raman analysis. IGZO films displayed a dramatic improvement in the surface morphology as compared with the single dopant films due to the compensation effect of gallium and indium doping which reduced the lattice strain. The XPS analysis confirmed the presence of the oxidized dopants in each film. All thin films have shown excellent optical properties with more than 90% transmission in the visible range of light. The blue-shift of the absorption edge accompanied by the increase of the optical band gap confirmed the Burstein–Moss effect. The UV PL peak originated from the near band edge emission of crystalline ZnO, while the visible PL was associated with the radiative transition related to oxygen interstitial (O_i) defects in the ZnO structure.

Keywords. ZnO; co-doping; RF sputtering; XPS; photoluminescence.

1. Introduction

Zinc oxide (ZnO) is a direct band gap (~3.37 eV at room temperature) material and has a large exciton binding energy (B.E.) of 60 meV; hence it is widely used as an optoelectronic material [1,2]. Many other properties such as biocompatibility, thermal stability and relatively simple and low-cost production make it useful in a wide range of applications such as transparent conductive oxide for solar cells, three-dimensional memory elements, thin film transistors, sensors, photo-detectors and light emitting diodes (LEDs) [3,4]. Doping of ZnO with suitable dopants is a well-known method for achieving the desired material properties. The idea of co-doping is not new. Co-doping allows the benefits of two dopants to be exploited simultaneously. The strengths of one dopant can compensate for the weaknesses of another. Many dopants have been used to improve the physical properties of ZnO. The most common of these are the group 13 elements such as aluminium [5], gallium [6], indium [7], etc.

Some related studies based on Al and Ga co-doped ZnO nanostructures *via* a sol–gel route to modify their electrical and sensing properties have been carried out by Hayder *et al* [8]. While Benhaliliba *et al* [9] synthesized ZnO thin films which were doped separately with Al and In and these films exhibited good electrical conductivity and high optical transmittance in the visible region. These trivalent elements by replacing the Zn atom in the parent crystal structure modify the ZnO lattice and reveal improved properties. And also these dopants are introduced as substitutional defects on zinc sites. The fact that the radius of 4-coordinate Ga³⁺ (0.62 Å) and that of In³⁺ (0.81 Å) is closer to that of 4-coordinate Zn²⁺ (0.74 Å), make it useful as a codopant for ZnO structures [10,11]. Thin film deposition of ZnO can be carried out by various techniques like sputtering [12], pulsed laser deposition [13], microwave assisted synthesis [14], sol–gel [15], ultrasonic spray pyrolysis [16], chemical bath deposition [17], etc. Among these, radio frequency (RF) sputtering is more suitable for high quality and large area deposition.

In this paper, pristine ZnO, indium-doped (IZO), gallium-doped (GZO) and indium and gallium co-doped ZnO (IGZO) thin films were deposited *via* RF sputtering techniques. All three of these materials were synthesized under the same conditions, which have allowed for an unprecedented and thorough comparison of the three doped materials. The effects of doping were investigated with respect to the crystal and grain growth of the films, and the resultant luminescence properties.

2. Experimental

2.1 Film preparation

Thin films of pristine ZnO, ZnO with In ($\text{Zn}_{0.99}\text{In}_{0.01}\text{O}$) (IZO) and Ga ($\text{Zn}_{0.99}\text{Ga}_{0.01}\text{O}$) (GZO) as a single dopant and indium and gallium ($\text{Zn}_{0.98}\text{In}_{0.01}\text{Ga}_{0.01}\text{O}$) (IGZO) as co-dopants were deposited on glass substrates using RF magnetron sputtering using powder targets. Sputter targets were prepared using a mixture of high purity ZnO powder and the desired amount of high purity In_2O_3 and Ga_2O_3 powders. The mixture was ground thoroughly, spread on a copper holder and pressed using a stainless steel puncher. Prior to the deposition of films the glass substrates were ultrasonically cleaned with trichloroethylene, acetone, methanol and deionized water for 10 min each. The cleaned substrates were dried in air before being introduced into the sputtering chamber. The chamber was evacuated to a base pressure of 3×10^{-5} mbar, and the substrates were then heated to a growth temperature of 100°C . A mixture of high purity Ar and O_2 gas (99.99%) was used as the plasma source, and the gas flow rate was controlled at 20 sccm each using a mass flow controller. A RF power of 75 W and a working pressure of 1.5×10^{-2} mbar were used for film deposition. The film deposition was carried out for 120 min and prior to the deposition pre-sputtering was carried out for 10 min to remove any contamination from the substrate.

2.2 Characterization of the film

The crystallinity of the films was examined by X-ray diffraction (XRD) using a D8 ADVANCE diffractometer. The surface morphology of the films was investigated by field emission scanning electron microscopy (FESEM, Make-Nova) and the attached energy dispersive X-ray spectroscopy (EDS) was used to examine the lateral variation of the elements. The photoluminescence (PL) spectra were recorded by using a fluorescence spectrometer (FLSP 920, Edinburgh Instruments). The chemical states of the films were identified by using an X-ray photoelectron spectrometer (XPS) using Mg- $K\alpha$ X-ray beams as the excitation source (1253.6 eV) and a DESA-150 electron analyser (Staub Instruments, Germany). Optical spectra were recorded using a UV-Vis Jasco V-530 in the wavelength range of 300 to 900 nm. Raman spectroscopy was performed using a Vyon Labram HR800 Raman spectrometer with the 632 nm excitation line of a solid state laser in the range of $100\text{--}800\text{ cm}^{-1}$. All the measurements were performed at room temperature.

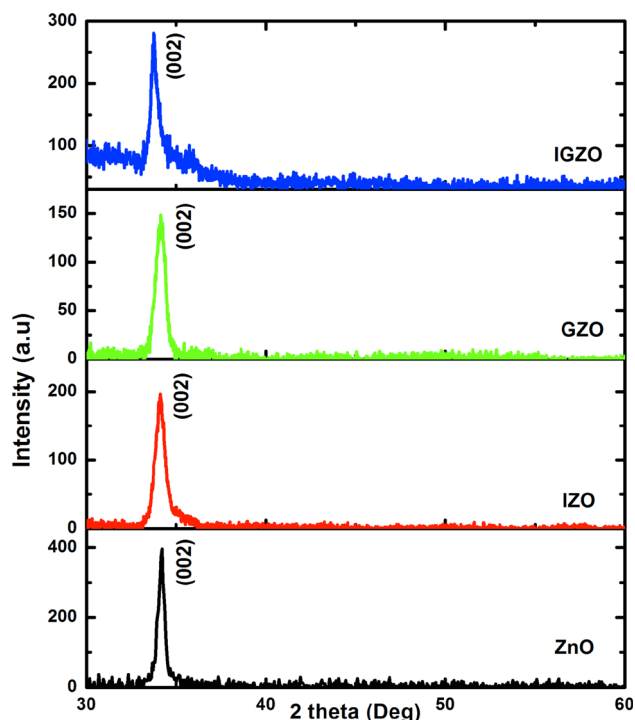


Figure 1. XRD patterns of pristine ZnO, IZO, GZO and IGZO nanocrystalline thin films.

3. Results and discussion

3.1 Phase composition and microstructure

The XRD patterns of pristine, single-doped (IZO and GZO) and co-doped (IGZO) ZnO thin films have only one strong (002) peak indicating that all films have a well-developed wurtzite structure and a good *c*-axis orientation perpendicular to the substrate (figure 1). No other peaks belonging to either gallium or indium phases are observed in the spectra, suggesting that both Ga and In are incorporated well into the ZnO lattice. It is observed that the doped-film shows a slight shift towards a lower angle compared to pristine ZnO, which can be attributed to the difference in the ionic radius of In^{3+} (0.81 Å), Ga^{3+} (0.62 Å) and Zn^{2+} (0.74 Å), respectively [18]. Also different shift directions of the (002) peak indicate different alternations of interplanar distances. The size of the crystallites (grain diameter) D was calculated using Scherrer's formula [19]:

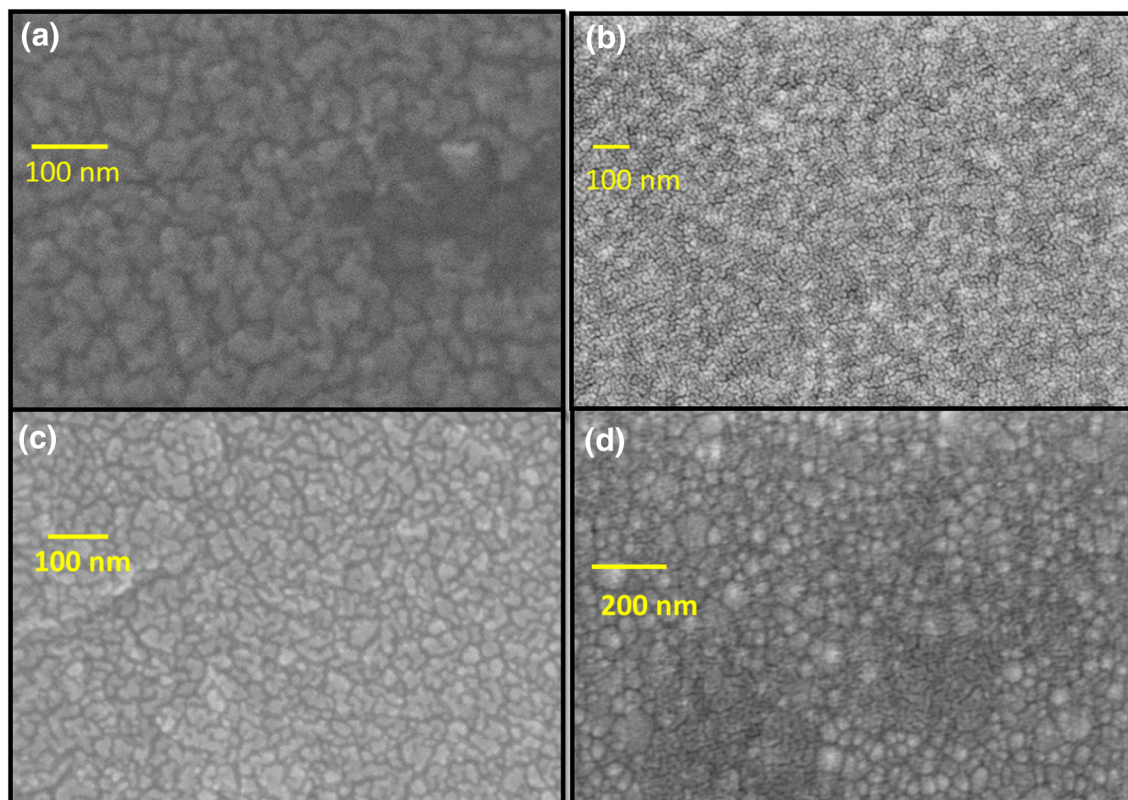
$$D = k\lambda/\beta \cos \theta, \quad (1)$$

where k is the shape factor generally taken as 0.9, λ is the wavelength of X-ray, β is the full-width at half maximum (FWHM) value and θ is the XRD peak position. The values of lattice parameters (a and c) of the hexagonal wurtzite structure were calculated from the XRD peak using the equation [19]:

$$a = \lambda/\sqrt{3} \sin \theta, \quad c = \lambda/\sin \theta, \quad (2)$$

Table 1. Lattice parameters of single and co-doped ZnO thin films calculated along the (002) orientation.

Sample	2θ	FWHM	D (Å)	Dislocation density (δ) $\times 10^{15}$	a (Å)	c (Å)	d (Å)	c/a	Strain (10^{-3})
ZnO	34.17	0.469	177	3.19	3.026 ± 0.004	5.241 ± 0.008	2.621 ± 0.004	1.732	1.96
IZO	34.12	0.729	114	7.70	3.031 ± 0.002	5.249 ± 0.004	2.625 ± 0.002	1.732	3.04
GZO	34.13	0.676	123	6.62	3.029 ± 0.003	5.248 ± 0.005	2.624 ± 0.003	1.732	2.82
IGZO	33.81	0.759	109	8.38	3.057 ± 0.006	5.295 ± 0.007	2.648 ± 0.008	1.732	3.17

**Figure 2.** FESEM micrograph of: (a) ZnO, (b) IZO, (c) GZO and (d) IGZO nanocrystalline thin films.

where values of a and c were estimated to be 3.026 and 5.248 Å, respectively, with a c/a ratio of 1.732.

The average lattice strain (ϵ) of the single and co-doped ZnO thin films can be obtained from the following expression [20]:

$$\epsilon = \beta \cos \theta / 4. \quad (3)$$

And the dislocation density (δ) is calculated from the relationship [20]:

$$\delta = 1/D^2. \quad (4)$$

The grain size and lattice parameters, dislocation density and strain developed in the film are tabulated in table 1.

It can be observed that the crystallite size of single and co-doped ZnO decreases from 177 to 109 Å. This could be attributed to the presence of a small strain and dislocations in the ZnO films due to the difference in the ionic radius of In (0.81 Å) and Ga (0.62 Å) dopants. The data reveal that the presence of In and Ga ions in ZnO prevents the growth of crystal grains. The calculated crystal defect parameters like microstrain and dislocation density indicate an increasing trend with doping while the crystallite size decreases due to the replacement of Zn^{2+} (0.74 Å) by In^{3+} (0.81 Å) and Ga^{3+} (0.62 Å). In the case of IGZO, it is possible that the simultaneous incorporation of both dopants in the lattice structure is leading to a compensation effect, and the difference in the size of the two dopants helps in reducing some of the crystal strain, in turn allowing greater dopant incorporation in the ZnO structure.

Figure 2 shows the FESEM images of pristine and doped-ZnO films. All the films have a dense, uniform, smooth and crack free microstructure. The morphology of ZnO and GZO has a granular structure while that of IZO shows a corn-like structure. The grain size of the IGZO thin films is smaller than that of ZnO which is attributed to the various relationships between the nucleation, growth and activation energy of the thin films [18,20]. The ionic radius inequality between Ga^{3+} (0.62 Å), In^{3+} (0.81 Å) and Zn^{2+} (0.74 Å) in the lattice site of ZnO has played a decisive role in the overall surface morphology modification of the films. Owing to the close ionic radius disparity between Ga^{3+} and In^{3+} , the compression in the volume caused by gallium to the ZnO lattice is effectively compensated and counteracted by the tension in the lattice caused by indium such that there will be less strain imposed in the lattice and fewer dislocations will be formed [20]. As a result, IGZO films have a better surface morphology than other films.

3.2 Elemental analysis

The weight % of all elements of the thin films is studied with the help of EDS and is summarized in table 2. The

Table 2. Compositional ratio of ZnO, IZO, GZO and IGZO thin films from EDS.

Sample	Zn (wt%)	O (wt%)	In (wt%)	Ga (wt%)	Total %
ZnO	52.2	47.8	—	—	100
IZO	68.8	29.5	1.7	—	100
GZO	58.6	41	—	0.4	100
IGZO	81.4	18	0.4	0.2	100

associated spectra obtained by EDS studies of all films are shown in figure 3a–d. EDS studies confirm the presence of doped elements such as In and Ga in ZnO. The amount of the doped elements are found to be less than the actual amount of target composition.

In order to understand the oxidation states of the deposited thin films, XPS analyses are performed and shown in figures 4 and 5. The spectra are corrected using the C 1s line from adventitious aliphatic carbon (285 eV). It is seen that the O 1s and Zn 2p peaks of the doped-ZnO thin films (figure 4a and b) shift towards higher B.E.s compared to pristine ZnO thin films. This attributed to the formation of stronger bonds between the dopants (In and Ga) and oxygen in doped-thin films compared to those between Zn and oxygen in the pristine ZnO. The B.E. of the zinc $2p_{3/2}$ and $2p_{1/2}$ peaks (figure 4b) of all the films is consistently found to be 1020.2 ± 0.2 and 1043.2 ± 0.2 eV respectively which can be attributed to Zn^{2+} in ZnO. The O 1s spectra of all the films can be deconvoluted into three distinct sub peaks (I, II and III) using Gaussian fitting (figure 4a). Among them, the low energy (region I) peak (529.4 ± 0.2 eV) originates from O^{2-} ions forming bonds with the metal cations (Zn^{2+} , In^{3+} and Ga^{3+}) in the lattice. The medium energy region II (530.4 ± 0.5 eV) components are associated with O^{2-} ions near the oxygen deficient regions within the ZnO lattice and region III (532.01 ± 0.5 eV) is due to the presence of loosely bound oxygen on the film surface belonging to a specific ratio such as CO_3 , adsorbed H_2O or adsorbed oxygen [14,21–23]. The In 3d and Ga 3d peaks are clearly seen from the XPS survey spectrum of IZO, GZO and IGZO thin films, indicating that In and Ga have indeed blended into the ZnO lattice. The gallium $3d_{5/2}$ peaks of GZO (figure 5b) and IGZO films (figure 5c) have B.E. of 20.33 and 20.31 eV, respectively, which is due to Ga^{3+} . Similarly, the indium $3d_{5/2}$ and $3d_{3/2}$ peaks of IZO (figure 5a) and IGZO

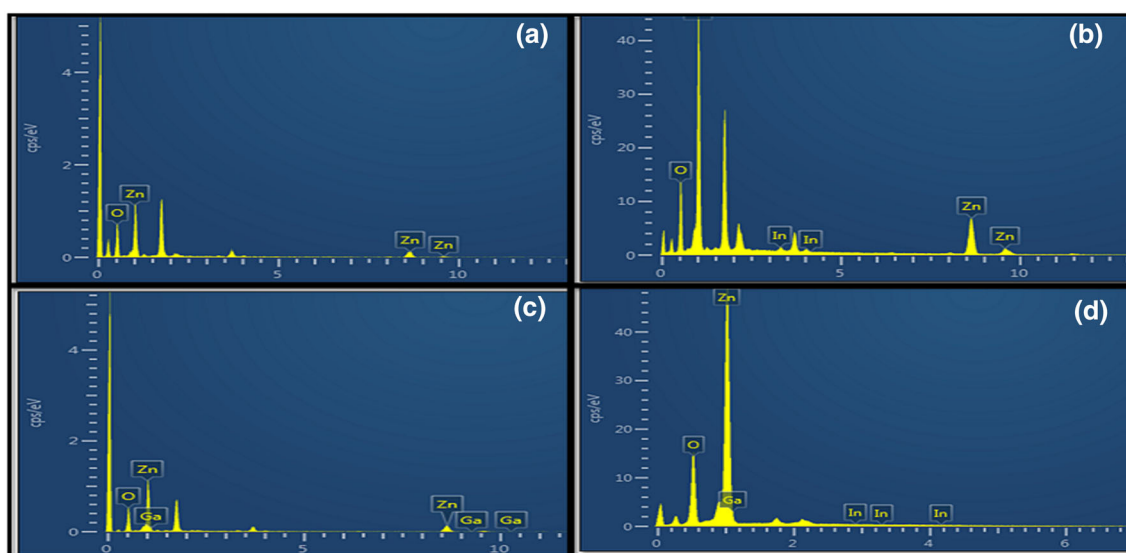


Figure 3. EDS spectra of: (a) ZnO, (b) IZO, (c) GZO and (d) IGZO nanocrystalline thin films.

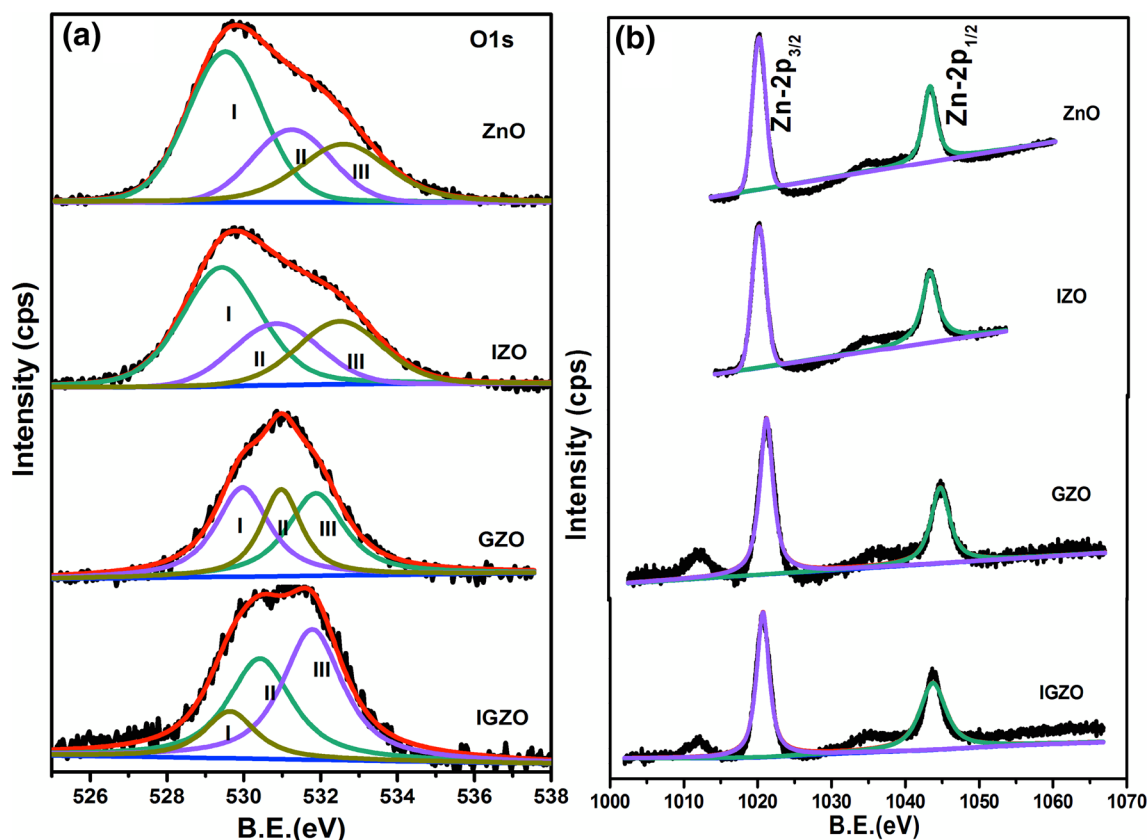


Figure 4. XPS analysis: (a) deconvoluted O 1s spectra and (b) Zn 2p spectra of ZnO, IZO, GZO and IGZO thin films.

(figure 5d) have B.E. of 444.4 and 451.5 eV and 444.9 and 452.29 eV respectively, which is due to In^{3+} [14].

3.3 Optical properties

The optical absorbance spectra of ZnO, IZO, GZO and IGZO thin films are shown in figure 6a. The well distinguishable peak in the UV range of the absorbance spectrum may be due to the exciton band of ZnO. The optical transmittance spectra of the deposited films are shown in figure 6b. All deposited films exhibit an average transmittance of $>90\%$ in the visible region and a sharp cut off between 360 and 375 nm. The transmittance at 540 nm of ZnO, IZO, GZO and IGZO films is found to be 80, 95, 89 and 83%, respectively. Among all the films, IZO shows the highest transmittance. It is evident that doping affects the transmittance of the films only marginally. This may be due to the formation of a grainy surface leading to the large scattering loss. The absorption edge of the IGZO film is shifted towards a lower wavelength. This shift is responsible for the improved transmittance in the lower wavelength region as compared to that of the pristine ZnO thin films. An interference fringe can be observed in each spectrum, indicating that the deposited films have a very smooth and homogeneous surface.

The optical band gap (E_g) of ZnO, IZO, GZO and IGZO thin films is computed using linear extrapolation of $(\alpha h\nu)^2$ vs. $h\nu$ plot. The absorption coefficient α has been calculated using Lambert's law for directly allowed transition [24]

$$(\alpha h\nu)^2 \propto (h\nu - E_g)^{1/2}, \quad (5)$$

where $h\nu$ is the incident photon energy and E_g is the optical band gap. The optical band gap of the films is found to be dependent on the doping. The band gap of IZO (3.20 ± 0.02 eV) and IGZO (3.16 ± 0.04 eV) films decreases (red shift) whereas for GZO films (3.31 ± 0.03 eV) it increases (blue shift) as compared with that of ZnO (3.24 ± 0.01 eV). This variation could be due to the increase in the carrier concentration, known as the Burstein–Moss effect [25].

3.4 PL spectra

Figure 7a–d illustrates the room temperature PL spectra of pristine and doped-ZnO thin films for an excitation wavelength of 325 nm. The spectral peak of all the samples is broad in the range of 350–600 nm. This broad visible band is associated with deep level emissions due to intrinsic point defects and defect complexes in the film structure. The fitted PL spectra of IZO (figure 7b) and GZO (figure 7c) consist of

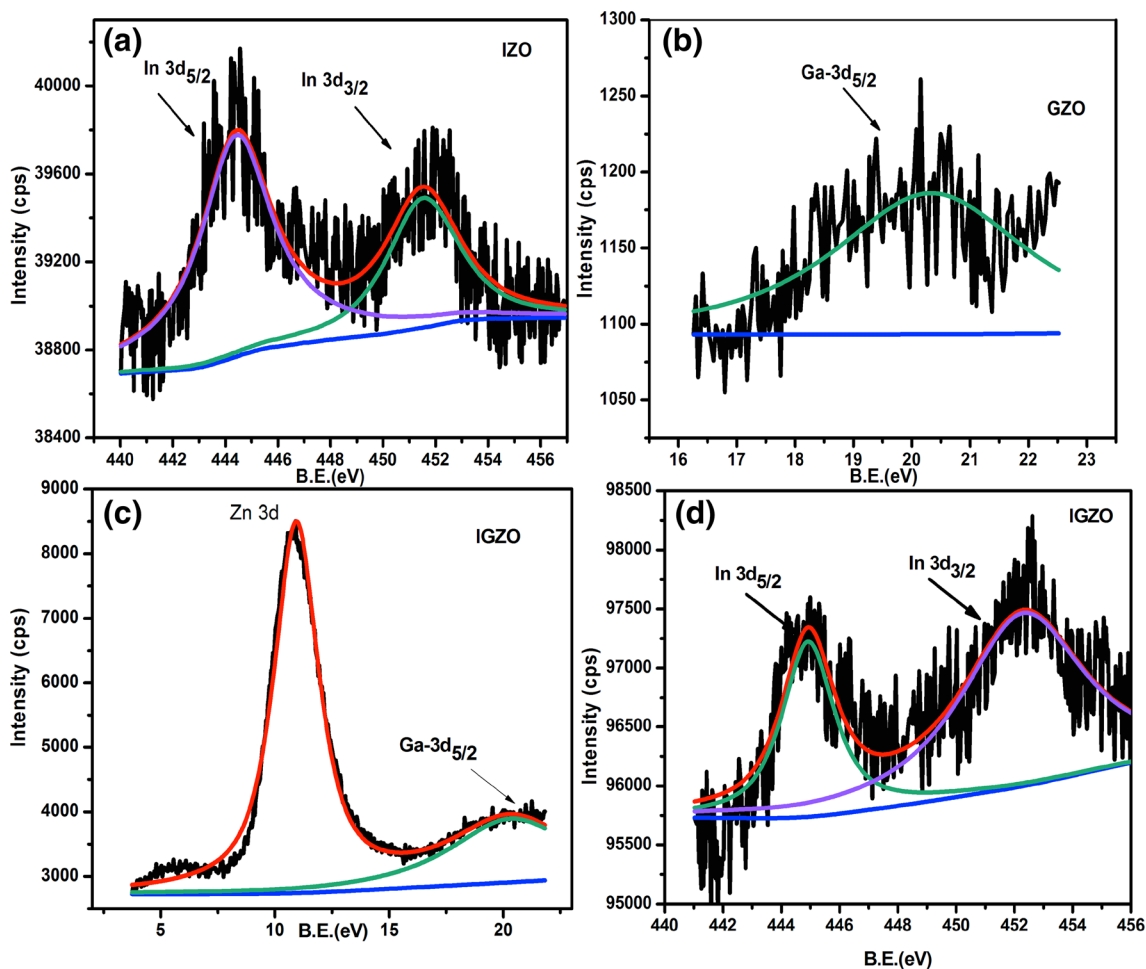


Figure 5. XPS spectra of: (a) In 3d in IZO, (b) Ga 3d_{5/2} in GZO and (c and d) In 3d and Ga 3d_{5/2} in IGZO thin films.

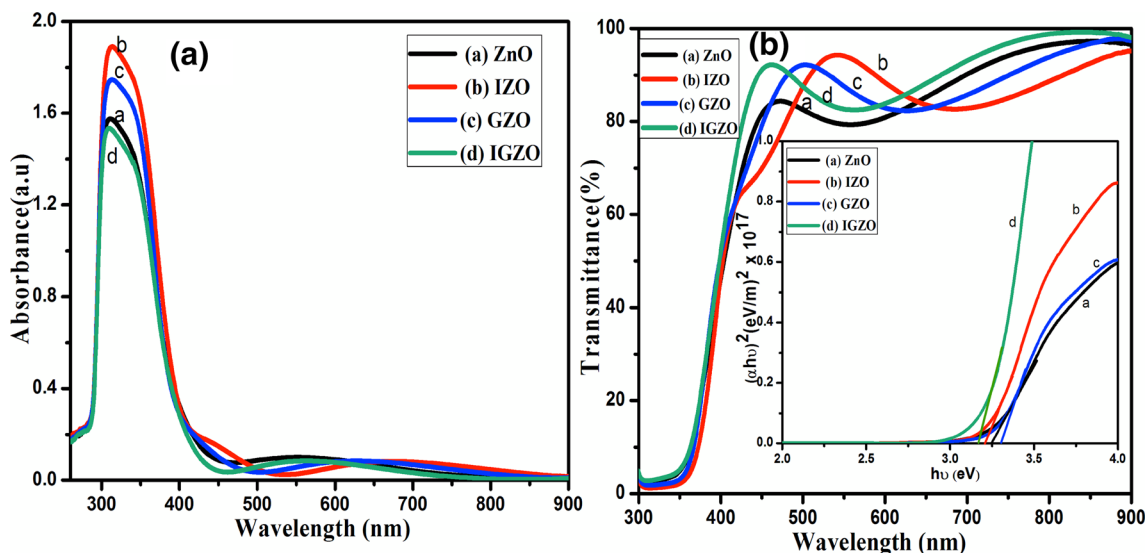


Figure 6. UV-visible (a) absorbance spectra and (b) transmittance spectra in the wavelength range of 300–900 nm and the inset shows the plot of $(\alpha h\nu)^2$ vs. $h\nu$ of the pristine, single and co-doped ZnO thin films.

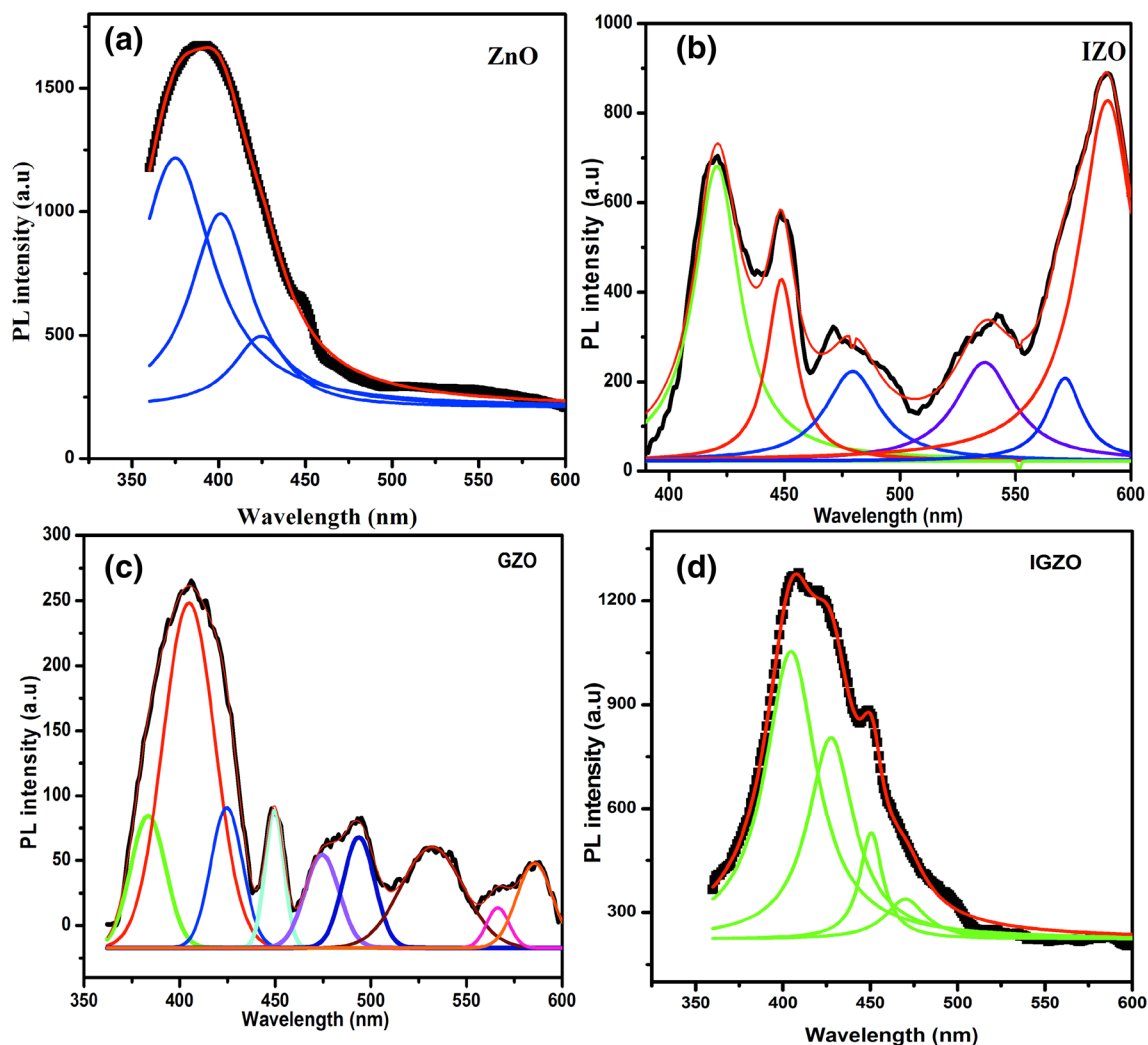


Figure 7. Deconvoluted room temperature PL spectra of (a) ZnO, (b) IZO, (c) GZO and (d) IGZO thin films (excitation at 325 nm).

several peaks. The orange–red emission is attributed to the deep interstitial oxygen (O_i) states inside the IZO structures. The yellowish–green emission is attributed to the transition from the bottom of the conduction of IZO and GZO structure to the O_i states, and the green emission is recognized as the V_O defects in both the structures [21]. The intensity of the orange–red emission is enhanced after indium doping, implying that the density of O_i states is increased in the IZO film. All the films exhibit the UV peak, which is associated with the free exciton–exciton collision process and is attributed to the near band edge emission (NBE) [26]. The pristine ZnO thin film exhibits an emission band ranging from 360 to 450 nm with a peak centred at 375 nm (figure 7a). For IGZO, (figure 7d) the emission band (ranging from 375 to 520 nm) is slightly shifted towards the visible region due to the incorporation of dopants with the peak centred at 420 nm. The PL spectra of IGZO thin films contain multiple peaks between 420 and 480 nm. These violet–blue and blue emissions are attributed to zinc interstitials (Zn_i) and zinc vacancy (V_{Zn}),

respectively, explaining the change in emission during doping [27,28]. From the PL characteristics, it is clearly evident that the co-doped IGZO material is a potential candidate for use in down converting LEDs.

3.5 Raman analysis

In order to crease information regarding the crystallinity and phase of the single and co-doped films, Raman measurement of the samples (on Si substrates) is taken. Figure 8a shows the Raman spectra of single and co-doped ZnO thin films. The Raman lines around 437 cm⁻¹ are observed for all the thin films, which is assigned to E2 (high) mode. This mode is assigned to the vibration of the oxygen sublattice and is the characteristics peak of the hexagonal wurtzite phase of ZnO films. In doped films, the E2 (high) mode is slightly blue-shifted from 437 to 436.4 cm⁻¹, caused by the tensile strain in the films which is in good agreement with the XRD result. A weak peak at 589 cm⁻¹ (figure 8b) corresponds to A1 (LO)

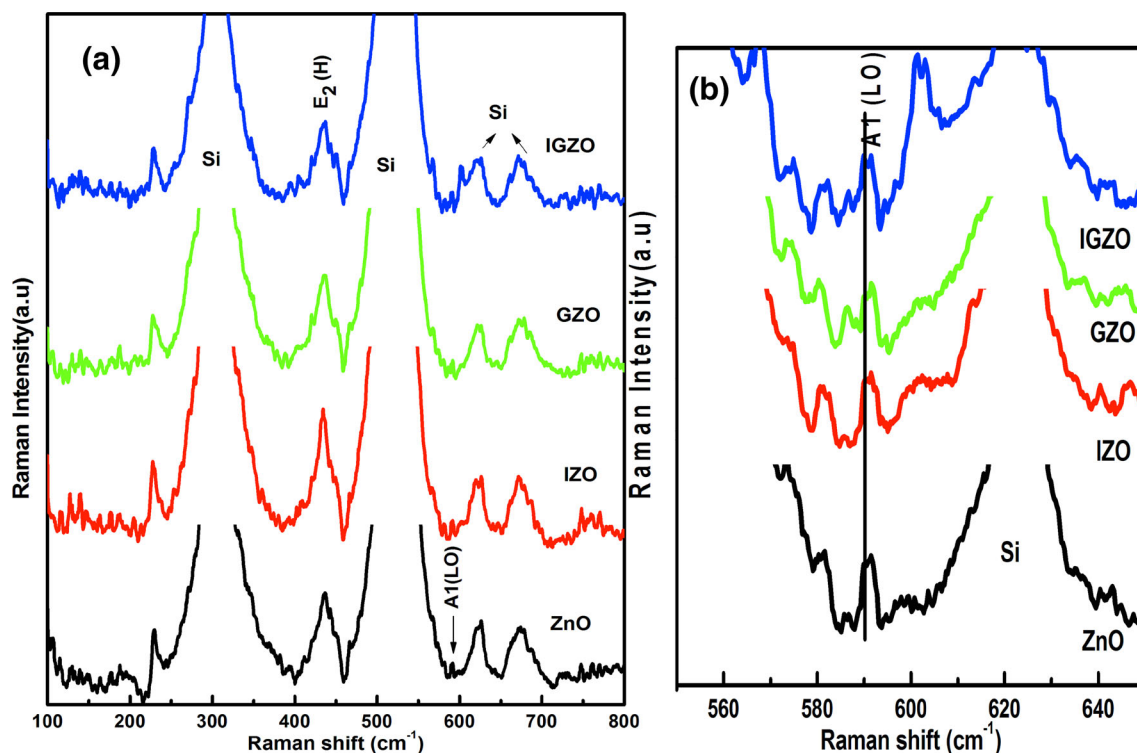


Figure 8. (a) Raman spectra and (b) enlarged view of single and co-doped ZnO thin films.

mode and may be caused by the defects such as O-vacancy and Zn interstitial and their complexes, which is consistent with the PL and XPS results.

4. Conclusion

Pristine, single (In, Ga) and co-doped ZnO thin films were deposited on glass substrates by RF magnetron sputtering. All the thin films exhibited a typical wurtzite structure with a strong (002) preferred orientation. XPS analysis confirmed the presence of the oxidized dopants in each film. The tensile strain in the films that caused the Raman line shift was in good agreement with that obtained from the XRD result. The peak attributed to the oxygen vacancy defect in Raman spectra is consistent with that observed from PL spectra and XPS. Among the doped films, the IGZO film showed better morphology, crystallinity and PL emission. All the films had very high-optical transmittance of the order of 95% in the visible range. The excellent optical properties reveal a great promise for the proposed thin films with applications in various optoelectronic devices.

Acknowledgements

The first and fourth authors would like to thank the thin film devices group, Technical Physics Division at BARC, Mumbai, for their help during the work.

References

- [1] Jayaraman V K, Alvarez A M, de la luz M and Amador O 2017 *Physica E* **86** 164
- [2] Wang F-H and Chang C-L 2016 *Appl. Surf. Sci.* **370** 83
- [3] Snigurenko D, Guziewicz E, Krajewski T A, Jakiela R, Syryanyy Y, Kopalko K *et al* 2016 *Mater. Res. Express* **3** 125907
- [4] Li X, Yang Y, Wu X, Zhang F C and Yang H 2018 *Ferroelectr.* **530** 11
- [5] Shahid M U, Deen K M, Ahmad A, Akram M A, Aslam M and Akhtar W 2016 *Appl. Nano Sci.* **6** 235
- [6] Castro M V and Tavares C J 2015 *Thin Solid Films* **586** 13
- [7] You H-C 2013 *Int. J. Electrochem. Sci.* **8** 9773
- [8] Al-Asedu H J, Bidis N, Al Khafaji S A and Bakhtiar H 2018 *Mater. Sci. Semicond. Proc.* **77** 50
- [9] Benhaliliba M, Benouis C E, Aida M S, Yakuphanoglu F and Sanchez Juarez A 2010 *J. Sol-Gel Sci. Technol.* **55** 335
- [10] Chang S-C 2014 *Nanoscale Res. Lett.* **9** 562
- [11] Chang S-C 2014 *Int. J. Photoenergy* **2014** 916189
- [12] Gaspara D, Pereira L, Gehrke K, Galler B, Fortunato E and Martins R 2017 *Sol. Energy Mater. Sol. Cells* **163** 255
- [13] Singh K, Dhar R and Mohan D 2016 *J. Integr. Sci. Technol.* **4** 33
- [14] Jayathilake D S Y, Nirmal Peiris T A, Sagu J S, Potter D B, Wijayantha K G U, Carmalt C J *et al* 2017 *ACS Sustain. Chem. Eng.* **5** 4820

- [15] Wahab H A, Salama A A, El-Saeid A A, Nur O, Willande M and Battisha I K 2013 *Results Phys.* **3** 46
- [16] Jayaraman V K, Álvarez A M, Kuwabara Y M, Koudriavstev Y, de la luz M and Amador O 2016 *Mater. Sci. Semicond. Proc.* **47** 32
- [17] Bidier S A, Hashim M R, Al-Diabat A M and Bououdina M 2017 *Physica E* **88** 169
- [18] Le H Q and Chua S J 2011 *J. Phys. D: Appl. Phys.* **44** 125104
- [19] Gadallah A S and El Nahass M M 2013 *Adv. Cond. Mat. Phys.* **2013** Article ID 234546
- [20] Rouchdi M, Salmani E, Fares B, Hassanain N and Mzerd A 2017 *Results Phys.* **7** 620
- [21] Chirakkara S and Krupanidhi S B 2011 *Phys. Status Solidi RRL* **6** 34
- [22] Wang F-H, Chao J-C, Liu H-W and Kang T-K 2015 *J. Nanomater* **2015** 936482
- [23] Duan J, Xiong Q, Hu J and Wang H 2015 *J. Power Energy Eng.* **3** 11
- [24] Zhu Y, Mendelsberg R J, Zhu J, Han J and Anders A 2013 *Appl. Surf. Sci.* **265** 738
- [25] Tohsophon T, Wattanasupinyo N, Silskulsuk B and Sirikulrat N 2013 *Thin Solid Films* **520** 726
- [26] Abbasi M A, Ibupoto Z H, Hussain M, Nur O and Willander M 2013 *Nanoscale Res. Lett.* **8** 320
- [27] Allabergenov B, Chung S-H, Jeong S M, Kim S and Choi B 2013 *Opt. Mater. Express* **3** 1733
- [28] Alvi N H, Ul Hasan K, Nur O and Willander M 2011 *Nanoscale Res. Lett.* **6** 130